Interdependence of Structure, Morphology and Phase Transitions in CVD grown VO_2 and V_2O_3 Nanostructures

David Graf, Johannes Schläfer, Simon Garbe, Axel Klein and Sanjay Mathur[*]

Institute of Inorganic Chemistry, University of Cologne

Greinstraße 6, D-50939 Cologne, Germany

(*corresponding author: sanjay.mathur@uni-koeln.de)

Keywords: vanadium alkoxides, CVD, vanadium oxides, nanostructured films

ABSTRACT

Phase selective chemical vapor deposition of nanostructured vanadium dioxide (VO_2) and sesquioxide (V_2O_3) was achieved by deploying $[V(OR)_4]_n$ (R = ^{t}Bu, n = 1 (**1**), R = Et, n = 3 (**2**), R = Me, n = 4 (**3**)). Use of $[V(O^tBu)_4]$ (**1**) produced thin films of monoclinic VO_2 (M1) at 700 and 800 °C consisted of anisotropic nanostructures with high crystallinity and small hysteresis in the metal-to-semiconductor transition (MST). Film morphologies manifested strong dependence on growth temperatures and exhibited pronounced texturing effects at high temperatures (>700 °C). The microstructure of the films was found to significantly affect the MST behavior of VO_2 films. DTA measurements of VO_2 films showed MST at 63 °C (700 °C) and 65 °C (800 °C), much lower than the transition temperature observed in single crystal material (68 °C). Precursors were characterized in the solid-state (XRD) and solution-state (temperature depended EPR, NMR) to reveal an association-dissociation equilibrium in solution (complex **2** and **3**), involving monomeric, dimeric and oligomeric species. Use of **2** and **3** as single precursors produced thin films of crystalline V_2O_3 consisting of nanosheets (5 nm) with a flower-like morphology.

1. INTRODUCTION

The binary V:O phase diagram consists of several homovalent and mixed-valent oxides (V_2O_5, VO_2, V_2O_3, V_6O_{13}) that exhibit distinctive electrical and optical properties interesting for various technological applications for thermochromic[1–4], catalytic[5], sensing[6] and electrode materials[7,8]. The rich variety of vanadium:oxygen stoichiometries emerge from the ability of vanadium atoms to adopt multiple oxidation states (+3, +4, +5), which in turn results in a synthetic challenge, when growing monophasic films of vanadium oxides.

Vanadium dioxide (VO_2) in particular has attracted a great deal of attention due to a temperature-dependent first order metal-to-semiconductor (MST) transition accompanied by a structural transformation (monoclinic structure VO_2 (M1) → tetragonal VO_2 (R)) manifested in an abrupt change in resistivity and near-infrared transmission.[9–11] Nevertheless, the implementation of vanadium dioxide films is still hampered by the high phase transition temperature (68 °C), accompanied by a large hysteresis and low visible light transmission in the semiconducting low-temperature state. Recent reports have shown that the phase transition temperature in VO_2 materials can be influenced by grain size and film morphology, as well as by electronic doping and strain induced phenomena.[12–15] Also V_2O_3 shows a reversible metal-to-insulator phase transition near 170 K from antiferromagnetic insulator to paramagnetic metal.[16] Both oxides are prototype compounds for Mott transition and of significant interest in condensed-matter physics due to their strongly correlated electron system.[17]

Vanadium oxide phases have been synthesized by several methods such as sol-gel[18], pulsed laser deposition[19], sputtering[20,21], atomic layer deposition (ALD) [22,23] or chemical vapor deposition (CVD)[24–27]. The synthesis of VO_2 (M1) films by aerosol-assisted and atmospheric pressure CVD has been extensively investigated mainly due to their easy

scalability, lower restriction on volatility of the precursors and easy introduction of dopants in films.[28–30] Nevertheless, the deposition of monoclinic VO_2 (M1) is only possible in a narrow temperature window around 550 °C and usually only a limited control over surface morphology has been observed.[26,31] Nanostructured surface morphologies play an important role in the thermochromic performance of VO_2 films in terms of phase transition temperature and visible light transmission.[32–34] Recently, Binions et al. reported the use of an electric field in an aerosol-assisted and atmospheric pressure CVD and demonstrated a reduction in the crystallite size and phase transition temperature.[35,36] A more common technique is the low pressure CVD, which allows a precise control of film texturing and composition, due to deposition temperature and proper choice of precursors.[37,38]

The common precursors for CVD of VO_2 thin films are vanadyl compounds (e.g. $[VO(acac)_2]$[31], $[VO(O^iPr)_3]$[24], $[VOCl_3]$[39]) that result in high halide and carbon contamination in the films, which accounts for leads to inferior electrical and optical properties. Vanadium (IV) alkoxides appear to be potential precursors for VO_2 thin films due to the preformed V–O bonds and preferred oxidation state (+4) of vanadium, however their utilization as precursor for CVD is not reported to the best of our knowledge.

Although the synthesis of homoleptic vanadium (IV) alkoxides has already been described by D. C. Bradley and M. L. Mehta,[40,41] more than 50 years ago there are still ambiguities concerning their molecular structures due to complex, temperature-dependent equilibria in solution and the gas phase. Recently, Soares et al.[42,43] observed a reversible thermochromic behavior for solutions of the dimeric complexes $[V(OR)_4]_n$ (R = ^{i}Pr, ^{neo}Pen, Cy) due to an association-dissociation equilibrium between a monomeric (blue) and a dimeric (green) species which highlights the importance of a comprehensive structural investigation of those complexes by complementary analytical techniques.

We report herein the solid-state structure of vanadium (IV) ethoxide $[V_3(\mu\text{-OEt})_4(OEt)_8]$ (**2**) and methoxide $[V_4(\mu\text{-OMe})_6(OMe)_{10}]$ (**3**) elucidated by single crystal X-ray diffraction studies and insight into their structural dynamics in solution from EPR and NMR spectroscopy. Moreover, the advantages of homoleptic vanadium (IV) alkoxides $[V(OR)_4]_n$ ($R = {}^t$Bu, $n = 1$ (**1**), R = Et, $n = 3$ (**2**), R = Me, $n = 4$ (**3**)) as molecular precursor for the phase-selective synthesis of vanadium oxides are demonstrated and the interdependence of morphology and growth temperature that influences the phase (structural) transitions is presented. The proper selection of molecular precursors and their tuning has an immense effect on the film composition and texture, which govern the efficacy of the opto-electrical properties of the as deposited layers.

2. RESULTS AND DISCUSSION

Precursor synthesis

The monomeric vanadium (IV) *tert*-butoxide $[V(O^tBu)_4]$ (**1**) was prepared according to the reported method, by reacting $[VCl_3(thf)_3]$ with four molar equivalents of lithium *tert*-butoxide in thf/*n*-heptane solution, followed by *in-situ* oxidation of the intermediate using copper (I) chloride.[44] The product was isolated by distillation as a highly volatile royal blue liquid. The addition of an excess amount of methanol or ethanol to a solution of $[V(O^tBu)_4]$ in toluene resulted in the formation of the respective homoleptic alkoxides indicated by a color change to green and finally to brown. The lower steric demand and higher pK_a value of the primary alcohols compared to those of *tert*-butanol allowed a complete ligand exchange reaction (Scheme 1).[43]

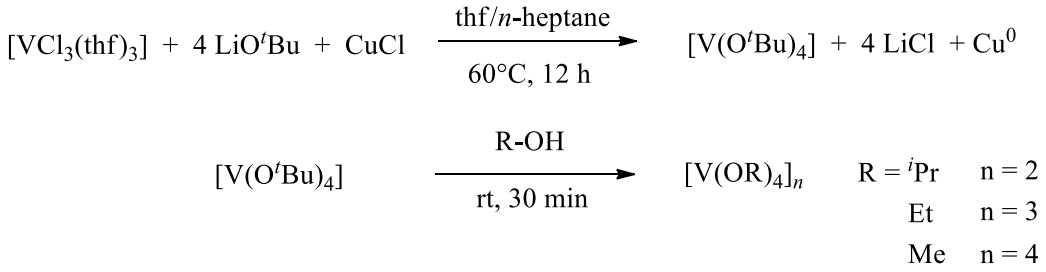

Scheme 1: Synthetic protocol of homoleptic vanadium (IV) alkoxides.

The homoleptic vanadium (IV) ethoxide complex (**2**) was isolated as a brown liquid, whereas the methoxide complex (**3**) has been obtained as a red-brown solid purified by distillation and recrystallization from a concentrated toluene solution, respectively.

Structural characterization of vanadium (IV) ethoxide and methoxide

Single crystal X-ray diffraction analysis (Table 1) of homoleptic vanadium (IV) ethoxide and methoxide complexes in the solid-state showed a trinuclear or tetranuclear framework, in $[V_3(\mu\text{-OEt})_4(OEt)_8]$ (**2**) and $[V_4(\mu\text{-OMe})_6(OMe)_{10}]$ (**3**), respectively. In (**2**) the central vanadium atom adopts a distorted octahedral coordination whereas the two peripheral vanadium atoms are coordinated in a distorted trigonal bipyramidal fashion. In (**3**) the two central vanadium atoms are symmetrically equivalent and their coordination is quite similar to the one in (**2**). The bridging alkoxo ligands showed in both complexes a typical elongation of the V–O bond distance (from 1.92(6) Å to 2.11(6) Å) compared to those of the terminal ligands (from 1.71(7) Å to 1.82(7) Å).[43] Moreover, the bridged alkoxo ligands exhibit an asymmetric bonding mode of the V–(μ-O*R*) bond distances to each vanadium center with short (1.92(6) Å; 1.96(6) Å) and long (2.08(6) Å; 2.11(6) Å) V–O distances. The nonbonding V–V distance in (**2**) was found to be 3.19(2) Å and the V–V–V angle 118.53(6)°.

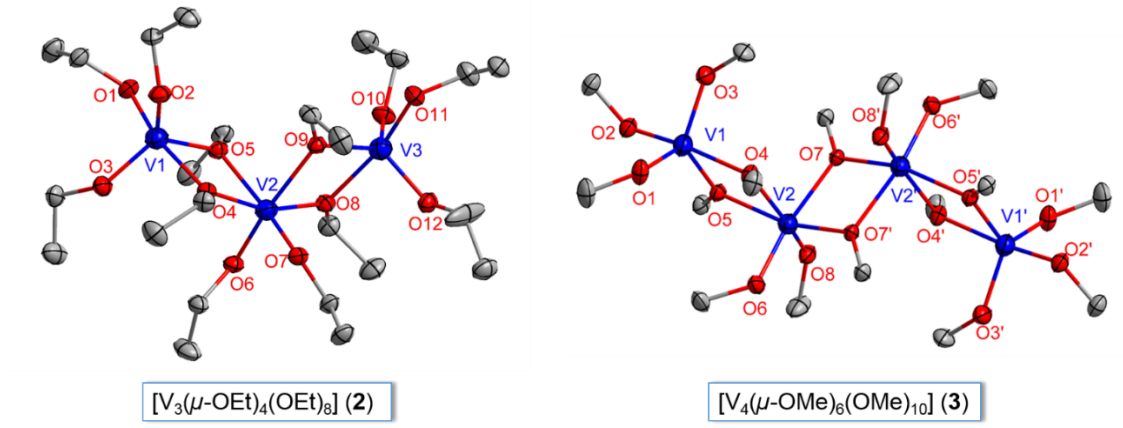

Figure 1: Molecular structures of $[V_3(\mu\text{-OEt})_4(OEt)_8]$ (left) and $[V_4(\mu\text{-OMe})_6(OMe)_{10}]$ (right). Thermal ellipsoids for V, O, and C atoms are shown at 30% probability level and the H atoms have been omitted for the sake of clarity.

Table 1: Details on crystal and structure refinement of vanadium (IV) ethoxide $[V_3(\mu\text{-OEt})_4(OEt)_8]$ (**2**) and methoxide $[V_4(\mu\text{-OMe})_6(OMe)_{10}]$ (**3**) complexes.

	$[V_3(\mu\text{-OEt})_4(OEt)_8]$	$[V_4(\mu\text{-OMe})_6(OMe)_{10}]$
Empirical formula	$C_{24}H_{60}O_{12}V_3$	$C_{16}H_{48}O_{16}V_4$
Formula weight / g mol^{-1}	693.54	700.31
T / K	170(2)	170(2)
Crystal system	triclinic	triclinic
Space group	$P\bar{1}$	$P\bar{1}$
a /Å	9.2267(7)	9.0432(7)
b /Å	12.9364(9)	9.4026(7)
c /Å	15.0845(1)	9.9726(7)
α / °	100.906(5)	85.999(6)
β / °	96.456(6)	68.051(5)
γ / °	96.384(6)	71.891(6)
V / Å^3	1740.5(2)	746.51(10)
Z	2	1
μ (Mo Kα) / mm^{-1}	0.839	1.277
No. of unique rflns, R_{int}	8142	5296

goodness of fit	0.870	1.061
final *R* indices [I > 2σ(I)]: R_1, wR_2	0.0489, 0.1014	0.0565, 0.1493
R indices (all data): R_1, wR_2	0.1145, 0.1240	0.0858, 0.1763
residual electron density	0.421, -0.620	0.855, -0.821

The equilibria between monomeric and oligomeric species in solution of vanadium (IV) methoxide and ethoxide complexes were analyzed by temperature depended EPR spectroscopy. Both complexes showed no visible thermochromic behavior. The EPR spectra of $[V_3(\mu\text{-OEt})_4(OEt)_8]$ were recorded in the solid-state as well as in toluene at room temperature, 225 K and in glassy frozen solution at 110 K (Figures 2 and S1 in the Supporting Information). The solid-state EPR spectra of vanadium (IV) ethoxide gave a strong broad signal at room temperature with no hyperfine structure (g_{iso} = 1.960, line-width A = 98 Gauss), whereas eight resonances of the isotropic hyperfine coupling were observed in the solution. The structural dynamics could be frozen at low temperatures so that the EPR spectrum at 110 K resembled the spectrum recorded in the solid-state at room temperature (Figure 2 insets). The hyperfine coupling apparently resulted from the presence of a mononuclear vanadium (IV) species (S = 1/2; ^{51}V, I = 7/2, 99.75% nat. abundance) in solution. Compared to the EPR spectra of the monomeric $[V(O^tBu)_4]$ (**1**) (Figure S1 in the Supporting Information, g_{iso} = 1.985, A = 70 Gauss), $[V_3(\mu\text{-OEt})_4(OEt)_8]$ (**3**) showed an asymmetric shape (g_{iso} = 1.970, A = 70 Gauss) with broad shoulders at 3100 and 3750 Gauss, arising from a ferromagnetic coupling between two vanadium atoms, which creates a triplet-state with a $\Delta M = \pm 1$ transition.[43] These observations suggest the presence of dimeric or/and trimeric species in the solution (Figure 2 and Scheme 2).

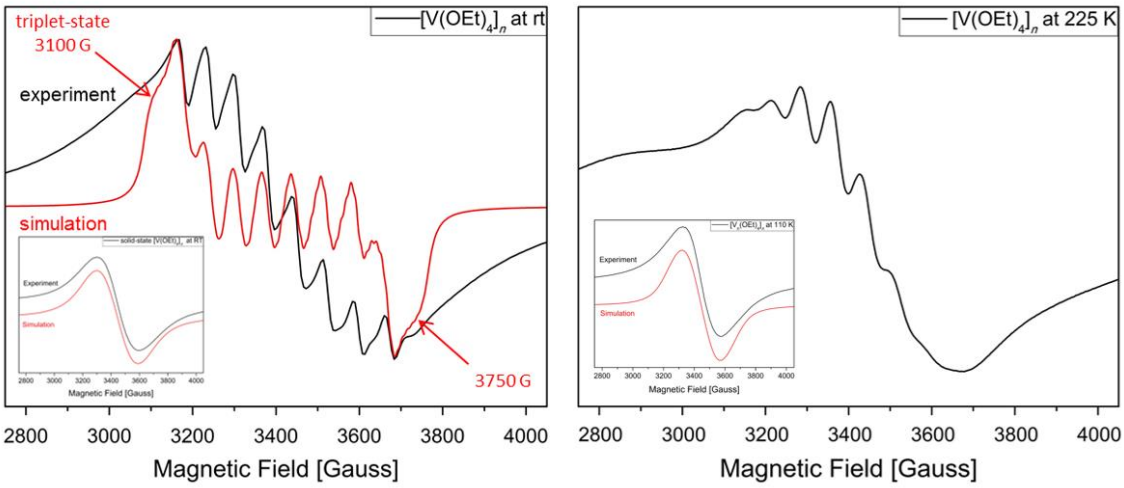

Figure 2: EPR spectra of $[V_3(\mu\text{-OEt})_4(OEt)_8]$ in toluene (left) in solid-state at room temperature (left inset) in toluene at 225 K (right) and 110 K (right inset).

The signal of the triplet-state was found to increase and the hyperfine coupling was blurred at 225 K, due to the lower molecular rotation and fluxionality. The EPR spectra at 110 K gave a broad intensive signal (g_{iso} = 1.962, A = 82 Gauss). When compared to $[V_3(\mu\text{-OEt})_4(OEt)_8]$, the EPR spectra of $[V_4(\mu\text{-OMe})_6(OMe)_{10}]$ did not show hyperfine pattern at room temperature (g_{iso} = 1.963, A = 97 Gauss), possibly due to the existence of several chemically distinct species in solution (Figures 2 inset and S1 in the Supporting Information).

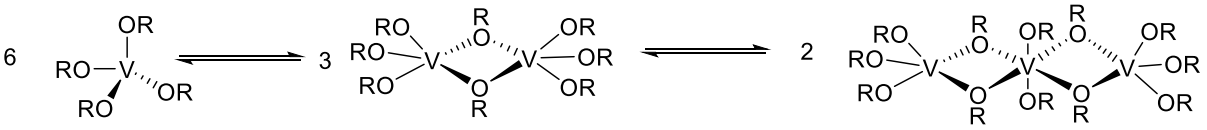

Scheme 2: Possible solution equilibria of $[V_3(\mu\text{-OEt})_4(OEt)_8]$.

^{51}V NMR spectroscopic measurements of $[V(OR)_4]_n$ (R = ^{t}Bu, n = 1 (**1**), R = Et, n = 2 (**2**), R = Me, n = 4 (**3**)) in toluene-d_8 at room temperature confirmed the presence of different vanadium species in solution (Figure 3). All vanadium (IV) alkoxides gave a singlet signal at

-676 ppm for a monomeric vanadium (IV) species while down field shifted signals indicated the presence of oligomeric vanadium (IV) species.

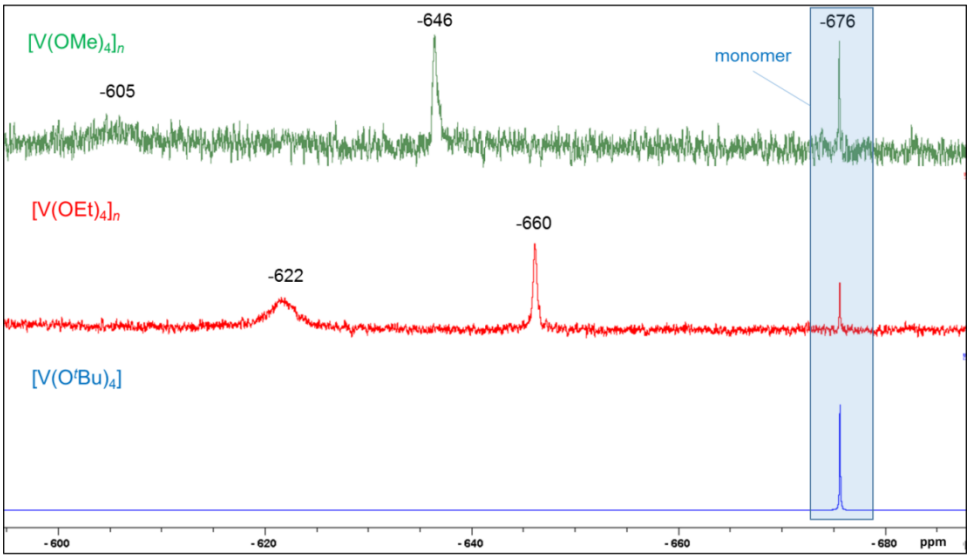

Figure 3: ^{51}V NMR spectra recorded in toluene-d_8 at room temperature of $[V(OR)_4]_n$ (R = ^{t}Bu, n = 1 (**1**), R = Et, n = 2 (**2**), R = Me, n = 4 (**3**)).

Synthesis and characterization of VO_2 and V_2O_3 thin films

Phase selective deposition of vanadium dioxide thin films on silicon and aluminum oxide substrates were achieved by vapor phase decomposition of $[V(O^tBu)_4]$ (**1**) in the temperature range at 500 to 800 °C. XRD analysis showed that pure monoclinic vanadium dioxide (M1) phase (PDF: 43-1051) was obtained at 700 and 800 °C, whereas mixed vanadium oxide phases were present at lower temperature (Figure 4). The diffractograms of the monoclinic VO_2 (M1) films exhibit varying intensity distributions for the (011) and (220) peaks whereas the (200) reflection is absent in all XRD pattern, which could be explained by preferred crystallite orientation on the silicon substrate. The XRD pattern of the films deposited at 500 and 600 °C could be assigned to different VO_2 phases and include some minor peaks which could not be assigned to any vanadium oxide phase.

The X-ray photoelectron spectroscopy (XPS) analysis showed that carbon contamination was higher in films deposited at lower temperature (Figure 4), probably due to incomplete

decomposition of precursor molecule and slow desorption of precursor fragments from the substrate. A short Ar^+-sputtering step (30 sec.) decreased the carbon content on the surface from 13.5 to 7.4 at% of VO_2 film grown at 750 °C, which displayed the origin of carbon from adsorbed organic molecules (Figure S5 in the Supporting Information).

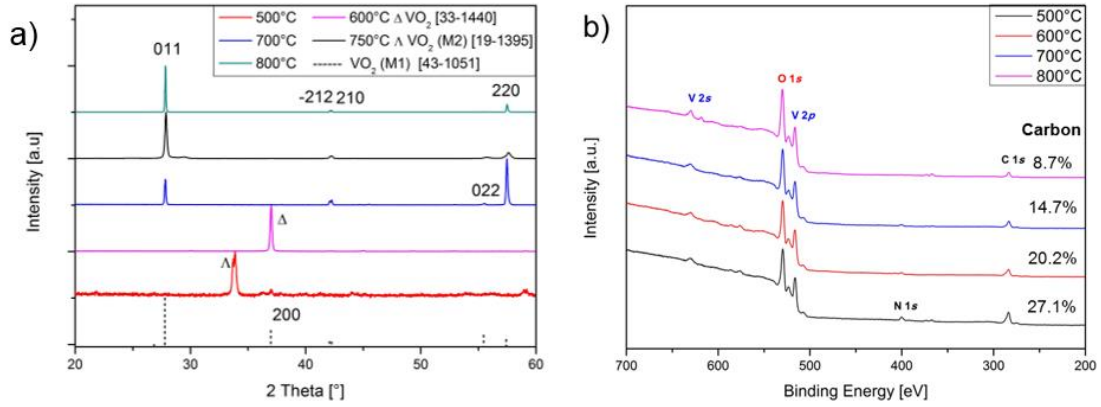

Figure 4: XRD patterns of the VO_2 films deposited in the temperature range at 500 to 800 °C (a). XPS spectra of vanadium oxides (b).

Scanning electron micrographs of the vanadium oxide films showed a significant temperature-dependent change in the surface morphology and microstructure (Figure 5). The films grown at 500 and 600 °C exhibited an island-like morphology with a columnar microstructure, possibly due to the low surface mobility of ad-atoms. Upon increasing the deposition temperature a denser and homogenous coating with facetted crystallites was obtained. At 700 °C, crystallites with one-dimensional structure were formed. The one-dimensional microstructure was confirmed by XRD data, which displayed a higher intensity of the (022) plane compared to film deposited at 750 and 800 °C. The film deposited at 800 °C consisted of sharp cuboidal crystallites with smaller grains ($d \approx 300$ nm) on the surface. It is noteworthy that anisotropic structures observed at 500 and 600 °C are transformed into dense microcrystals at 800 °C, possible due to sintering of one-dimensional grains.

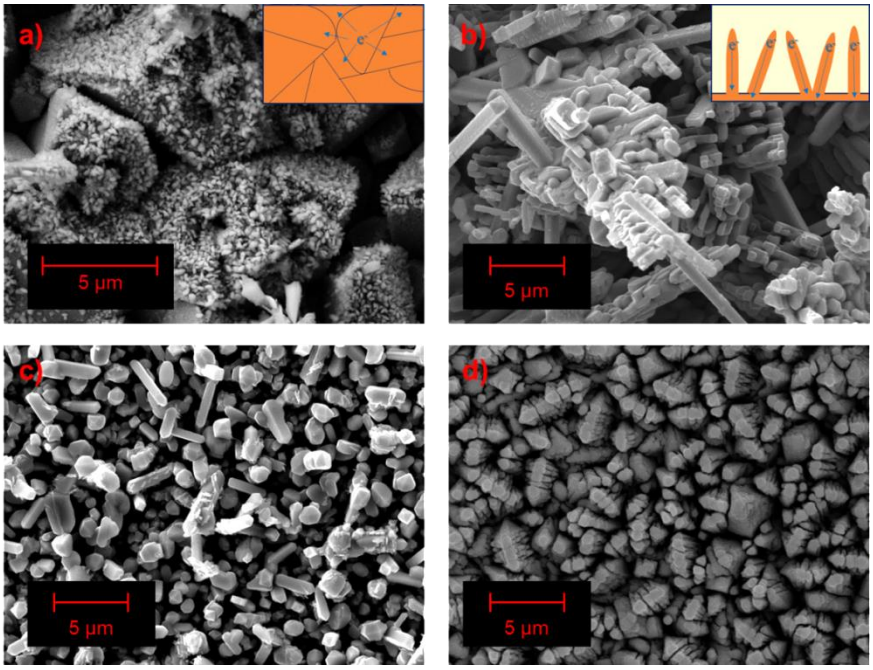

Figure 5: SEM micrographs illustrating the different surface morphology of vanadium dioxide films deposited on silicon for 30 min at 800 °C (a), 700 °C (b), 600 °C (c) and 500 °C (d). Insets (a) and (b) show the proposed charge mobility in the systems above.

Differential thermal analysis (DTA) measurements of the samples deposited at 700 °C and 800 °C for 30 min showed a reversible phase transition, from a semiconducting monoclinic phase to a metallic tetragonal phase (Figure 6). The transition temperatures (taken from the onset of the exothermic and endothermic peak) in both films (63 and 65 °C) was lower than that of bulk VO_2 (68 °C) and do not show typical hysteresis behavior. Moreover, the reversible phase transition was found to depend on the microstructure, since the film with one-dimensional crystallites showed a lower transition temperature (63 °C) and sheet resistance at room temperature (944.24 Ω/sq) than the film with cuboidal crystallites (65 °C, 2300.69 Ω/sq), probably due to enhanced directionality of charge carriers in vertically grown VO_2 grains (inset Figure 5 (a), (b)). It has to be noted that DTA measurements are not sensitive enough to determine the phase transition of thin VO_2 layers.

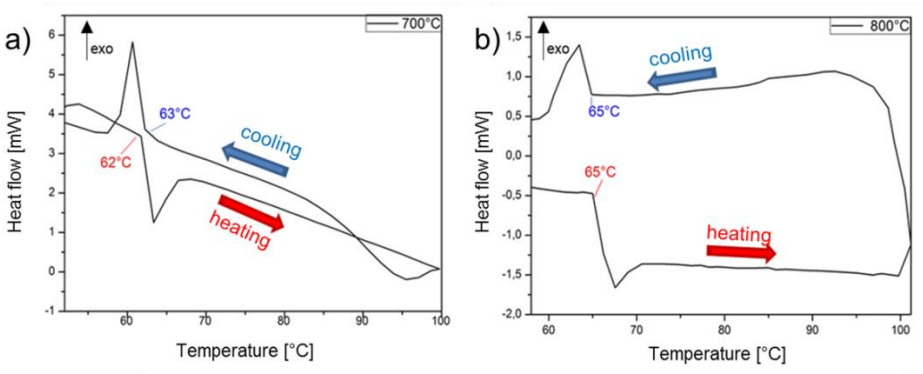

Figure 6: DTA measurement of vanadium dioxide films deposited on silicon for 30 min at 800 °C (a) and 700 °C (b).

For thermochromic window applications thin VO_2 films on glass with high transmittance are required. As an illustrative example, $[V(O^tBu)_4]$ (**1**) was deposited on glass at 700 °C for 1 min. The obtained thin VO_2 film (120 nm) showed a homogenous coating consisting of cuboidal crystallites (Figure S6 in the Supporting Information). Variable-temperature transmission UV/vis spectroscopy displayed a reversible phase transition around ca. 68 °C, consistent with undoped VO_2 thin film (Figure 7).[20,27] Large hysteresis (11 °C) and low solar transmission (T_{sol}: 1.46%) were obtained. The differences to the TG results could be explained by a substrate mediated strain-effects for the silicon substrates, which is known to reduce the transition temperature as well as reducing the hysteresis, probably due to surface oxidation of the VO_2 layer.[45,46]

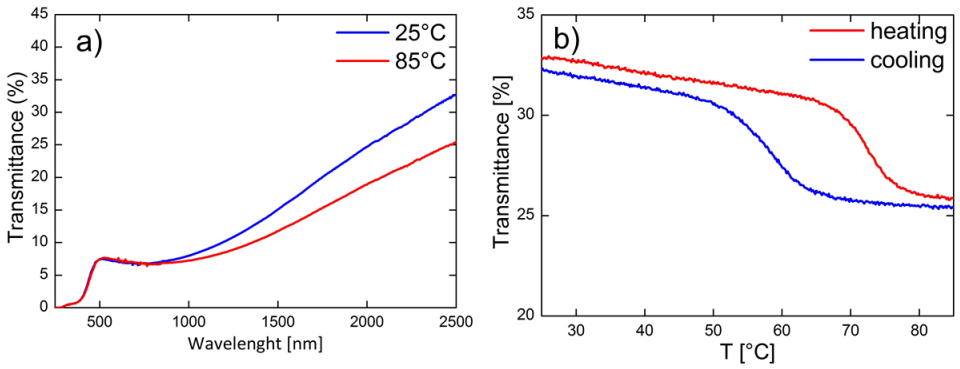

Figure 7: Transmission UV/vis spectra of vanadium dioxide films deposited on glass at 700 °C for 1 min (a) and temperature dependence of transmittance at 2500 nm (b).

The use of $[V_3(\mu\text{-OEt})_4(OEt)_8]$ (**2**) and $[V_4(\mu\text{-OMe})_6(OMe)_{10}]$ (**3**) in CVD on silicon and aluminum oxide resulted in V_2O_3 in both cases (Figure 8). The reduction of the vanadium (IV) in the precursor to vanadium (III) oxide could be achieved by the release of alcohol, ethanol and methanol, that react as reductant during decomposition. High resolution XPS spectra of V_2O_3 showed, upon fitting with sum of Gaussian-Lorentz functions, presence of V (III) (514.42 eV) and V (IV) (516.72 eV) centers in 4:1 ratio that were verified by reported data (Figure 8).[47,48]

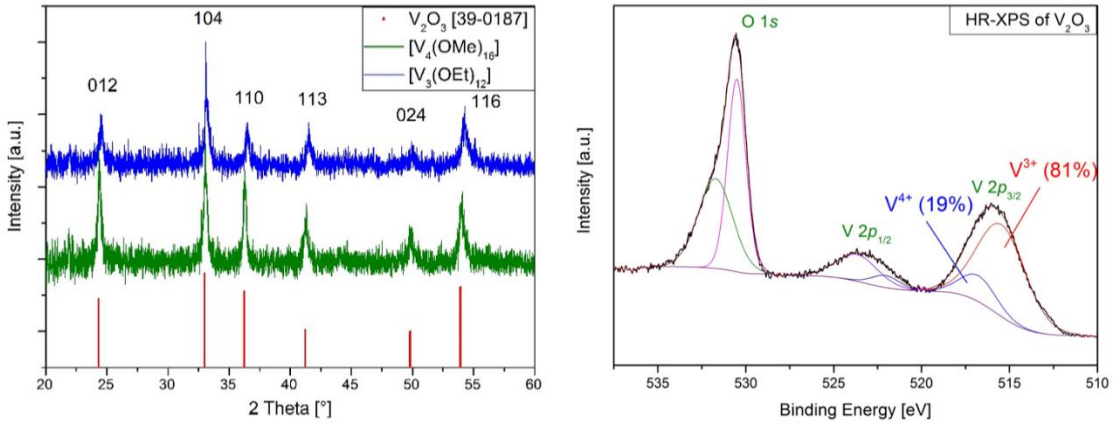

Figure 8: XRD pattern of vanadium sesquioxide V_2O_3 film deposited on silicon at 500 °C for 30 min using $[V_3(\mu\text{-OEt})_4(OEt)_8]$ and $[V_4(\mu\text{-OMe})_6(OMe)_{10}]$ as precursors (left). High resolution XPS spectra of V_2O_3 film synthesized from $[V_3(\mu\text{-OEt})_4(OEt)_8]$ (right).

The spectra displayed the typically two-peak structure (2 $p_{3/2}$ and 2 $p_{1/2}$) due to the spin–orbit splitting. The binding energies decreased with lower oxidation state of the vanadium atom. The presence of V (IV) in significant amount is likely due to the surficial oxidation of V_2O_3 films, which is difficult to avoid due to extreme sensitive nature of V (III) centers. The presence of VO_2 overlayer was also confirmed by HR-TEM studies (Figure 9 d).

In contrast to VO_2 films, the surface of V_2O_3 thin films deposited with (**2**) and (**3**) showed a unique morphology and dense structures by self-assembly of nanosheets with a thickness in between 50-100 nm (Figure 9). V_2O_3 thin films exhibited a low sheet resistance at room temperature of 46 Ω/sq and 80 Ω/sq, respectively, but slightly higher than epitaxially grown films on sapphire produced by oxygen plasma-assisted thermal evaporation (see Figure S7 in the Supporting Information).[49]

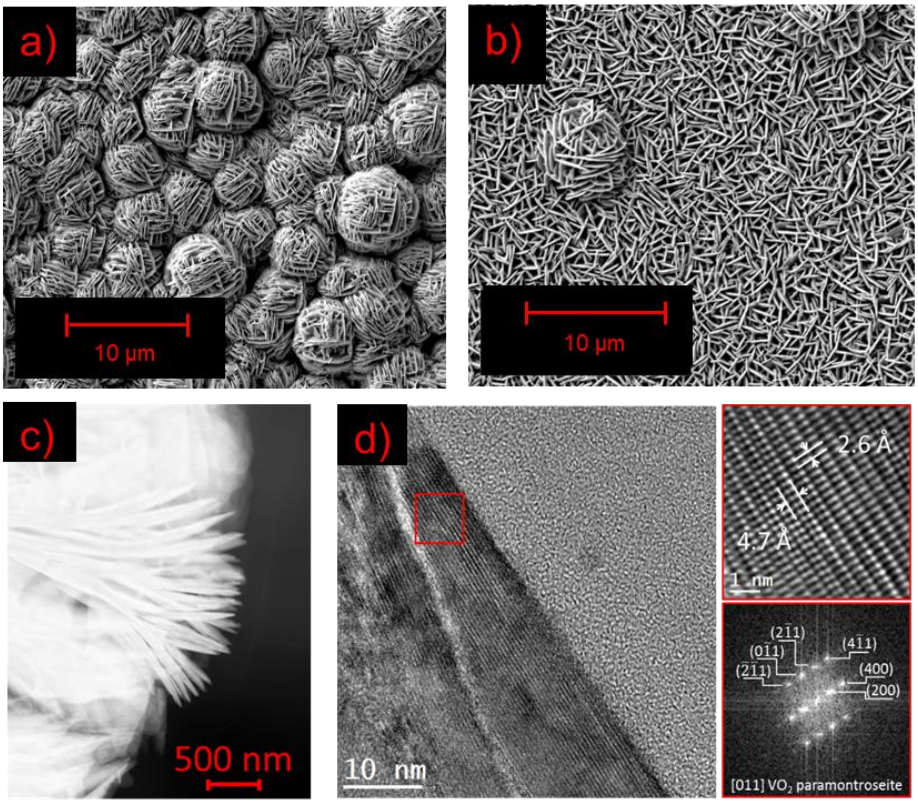

Figure 9: SEM micrographs of V_2O_3 thin films deposited on silicon with [$V_4(\mu$-$OMe)_6(OMe)_{10}$] (a) and [$V_3(\mu$-$OEt)_4(OEt)_8$] (b). Cross-section (c). HR-TEM micrograph taken from part of the vanadium oxide sheet. Magnified detail of the red square region and its corresponding power spectrum are shown on the right side (d).

Intriguingly, the aerobic oxidation of V_2O_3 films upon annealing in air resulted in the formation of biphasic mixture of V_2O_5 an V_3O_7 phases, which was confirmed by X-ray diffraction data (Figure 10). It is evident that the room-temperature oxidations of V_2O_3 films produced metastable VO_2 paramontroseite phase (Figure 9 d), whereas the accelerated oxidation at high temperatures (>500 °C) and resulted in the kinetically (V_3O_7) and thermodynamically favored (V_2O_5) phases. The room-temperature oxidations could be resulted by a hydrolysis to montroseite VO(OH) and subsequent oxidation in air (Figure 10).[50, 51]

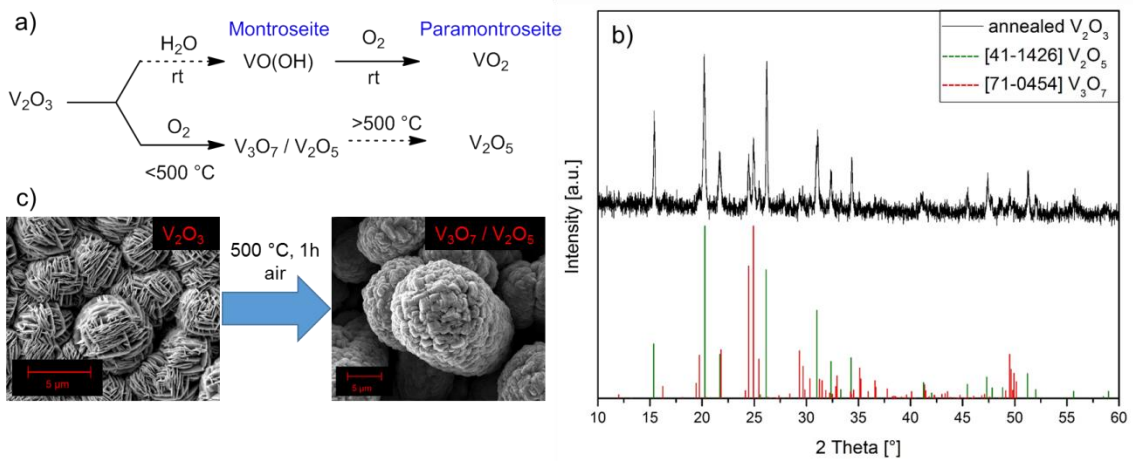

Figure 10: Reaction pathway of room-temperature and high temperature oxidation V_2O_3 films (a), XRD pattern of annealed V_2O_3 film (b) SEM micrograph of V_2O_3 and V_3O_7/V_2O_5 films (c).

3. CONCLUSION

Vanadium (IV) alkoxides are suitable precursors for phase-selective synthesis of VO_2 and V_2O_3 nanostructures due to their high volatility and low decomposition temperatures without using reactive gas. We demonstrated a strong dependence of substrate temperature on film morphologies to control the phase transitions by properly tuning the microstructures. The lowering of MST temperature (63 °C instead of 68 °C) in films grown at lower temperatures illustrates the effect of microstructure and grain anisotropy on the functional properties.

The strong influence of precursor on film properties were presented by using (**2**) and (**3**), which revealed an *in-situ* reduction by the released alcohol and resulted in an electric conductive V_2O_3 films with unique flower-like nanostructures.

4. EXPERIMENTAL

Precursor Synthesis

All manipulations of air and moisture sensitive materials were carried out under nitrogen using Stock-type all glass assemblies. X-band EPR spectra were recorded with a Bruker System ELEXSYS 500E instrument equipped with a Bruker ER 4131VT variable-temperature unit. Spectral simulation was performed by using Bruker SimFonia V1.26 software. NMR spectra were recorded on a Bruker Avance II spectrometer operating at 300 MHz, chemical shifts are quoted in part per million (ppm) relative to $VOCl_3$. Mass spectra were recorded on a Finnigan MAT 95 (EI, 20 eV) in m/z (intensity in %). UV/Vis absorption spectra were recorded with a Varian Cary50 Scan spectrophotometer. Data collection for X-ray structure elucidation was performed on a STOE IPDS I/II diffractometer using graphite-monochromated Mo Kα radiation (0.71071 Å). The programs used in this work are STOE's X-Area[52] and the WINGX suite of programs[53], including SIR-92[54], SHELX & SHELXTL[55] and PLATON[56] for structure solution and refinement. H-atoms were calculated geometrically and a riding model was applied during the refinement process.

[V(O^{t}Bu)$_4$] (**1**) was prepared following a procedure described by *Haaland et al*.[44] Yield: 63% (9.8 g). ^{51}V NMR (79.0 MHz, 298 K, Tol-d_8) δ: -676 (s). UV-Vis (*n*-heptane): λ_{max}= 722 nm (ε= 497 l mol^{-1} cm^{-1}), EI-MS (20 eV, 70° C): *m/z* (intensity) 343 (2%) [M]$^+$, 328 (10%) [M-CH$_3$]$^+$, 271 (40%) [M-O^{t}Bu]$^+$, 159 (100%).

[V$_3$(μ-OEt)$_4$(OEt)$_8$] (**2**). To a stirred blue solution of 1.0 g [V(O^{t}Bu)$_4$] (**1**) (2,9 mmol) in 5 mL toluene, 5 mL EtOH (86 mmol) was slowly added. This solution was stirred at ambient temperatures for 30 minutes and the colour changed from blue to green and finally to brown. The reaction mixture was evaporated to dryness and the crude product was purified by vacuum distillation (80 °C, 10^{-2} mbar). Yield: 1.6 g (1.94 mmol, 67%), ^{51}V NMR (79.0 MHz, 298 K, Tol-d_8) δ: -676 (s), -646 (s), -622 (bs). UV-Vis (*n*-heptane): λ_{max}= 719 nm (ε = 55 l mol^{-1} cm^{-1}), EI-MS (20 eV, 70° C): *m/z* (intensity) 215 (50%) [M]$^+$, 187 (100%) [M-OEt]$^+$.

[V$_4$(μ-OMe)$_6$(OMe)$_{10}$] (**3**). The synthetic procedure was similar to that described for **2**, starting from 1.0 g (2.9 mmol) of (**1**). The crude product was purified by vacuum sublimation (90 °C, 10^{-2} mbar). Yield: 1.4 g (1.97 mmol, 68%), ^{51}V NMR (79.0 MHz, 298 K, Tol-d_8) δ: -676 (s), -636 (s), -605 (bs), -676 (s), -646 (s), -622 (bs). UV-Vis (*n*-heptane): λ_{max}= 718 nm (sh) (ε= 9 l mol^{-1} cm^{-1}), EI-MS (20 eV, 90° C): *m/z* (intensity) 175 (4%) [M]$^+$, 145 (100%) [M-OMe]$^+$,130 (74%) [M-OC$_2$H$_6$]$^+$,113 (47%) [M-OC$_3$H$_9$]$^+$.

CVD Experiments

Thermal CVD. Experiments were performed in a horizontal hot-wall CVD reactor in which a high-frequency field was used to inductively heat the substrates by placing them on a graphite susceptor. The molecular precursors were introduced to the reactor through a glass flange by applying a dynamic vacuum (5*10^{-3} mbar) and heating the precursor reservoir to

the desired temperature. The precursor temperature was set to 35 °C for **1** and 60 °C for **2** and **3,** respectively.

Material Characterization. Room-temperature powder X-ray diffraction (XRD) was obtained on a STOE-STADI MP diffractometer operating in the reflection mode using Cu Kα (λ = 1.5406 Å) radiation. The microstructures of the samples were examined using field-emission scanning electron microscopy (FE-SEM, FEI Nova NanoSEM 430). X-ray photoemission spectroscopy (XPS) was performed on ESCA M-Probe (Al Kα) with an energy resolution of 0.8 eV). DTA measurements were performed on a TGA/DSC1 (METTLER-TOLEDO-GmbH, Germany) apparatus. I-V curves were measured with a 4-point probe setup. A Keithley 2400 SMU was used to record the I-V data. Data points were measured from −0.2 V to 0.8 V with a step size of 0.01 V. The UV-vis spectroscopy was performed in a water cooled peltier element cuvette holder. The temperature was kept constant at either 25 °C (blue line) or 85 °C (red line) while the steady state transmission spectrum was measured from 250 to 2500 nm with 5 nm intervals and slits. For the temperature scans the transmission was probed at 2500 nm with 5 nm slits while the temperature was ramped from 25 °C to 85 °C at 10 °C/min (red line).

Acknowledgment

The authors gratefully acknowledge Dr. Jordi Arbiol (ICREA and Catalan Institute of Nanoscience and Nanotechnology) for HR-TEM micrographs and Dr. Tero-Petri Ruoko (Tampere University of Technology) for temperature-dependent UV/vis spectroscopy. The University of Cologne is thanked for financial support.

5. References

(1) Warwick, M. E. A.; Binions, R. Chemical Vapour Deposition of Thermochromic Vanadium Dioxide Thin Films for Energy Efficient Glazing. *J. Solid State Chem.* **2014**, *214*, 53–66 DOI: 10.1016/j.jssc.2013.10.040.

(2) Aijaz, A.; Ji, Y.-X.; Montero, J.; Niklasson, G. A.; Granqvist, C. G.; Kubart, T. Low-Temperature Synthesis of Thermochromic Vanadium Dioxide Thin Films by Reactive High Power Impulse Magnetron Sputtering. *Sol. Energy Mater. Sol. Cells* **2016**, *149*, 137–144 DOI: 10.1016/j.solmat.2016.01.009.

(3) Gagaoudakis, E.; Kortidis, I.; Michail, G.; Tsagaraki, K.; Binas, V.; Kiriakidis, G.; Aperathitis, E. Study of Low Temperature Rf-Sputtered Mg-Doped Vanadium Dioxide Thermochromic Films Deposited on Low-Emissivity Substrates. *Thin Solid Films* **2016**, *601*, 99–105 DOI: 10.1016/j.tsf.2015.11.007.

(4) Granqvist, C.; Niklasson, G. Thermochromic Oxide-Based Thin Films and Nanoparticle Composites for Energy-Efficient Glazings. *Buildings* **2016**, *7* (1), 3 DOI: 10.3390/buildings7010003.

(5) Zavahir, S.; Xiao, Q.; Sarina, S.; Zhao, J.; Bottle, S.; Wellard, M.; Jia, J.; Jing, L.; Huang, Y.; Blinco, J. P.; Wu, H.; Zhu, H. Y. Selective Oxidation of Aliphatic Alcohols Using Molecular Oxygen at Ambient Temperature: Mixed-Valence Vanadium Oxide Photocatalysts. *ACS Catal.* **2016**, *6* (6), 3580–3588 DOI: 10.1021/acscatal.6b00753.

(6) Epifani, M.; Comini, E.; Siciliano, P.; Faglia, G.; Morante, J. R. Evidence of Catalytic Activation of Anatase Nanocrystals by Vanadium Oxide Surface Layer: Acetone and

Ethanol Sensing Properties. *Sensors Actuators B Chem.* **2015**, *217*, 193–197 DOI: 10.1016/j.snb.2014.07.118.

(7) Niu, C.; Huang, M.; Wang, P.; Meng, J.; Liu, X.; Wang, X.; Zhao, K.; Yu, Y.; Wu, Y.; Lin, C.; Mai, L. Carbon-Supported and Nanosheet-Assembled Vanadium Oxide Microspheres for Stable Lithium-Ion Battery Anodes. *Nano Res.* **2016**, *9* (1), 128–138 DOI: 10.1007/s12274-015-0896-6.

(8) Liu, Q.; Li, Z.-F.; Liu, Y.; Zhang, H.; Ren, Y.; Sun, C.-J.; Lu, W.; Zhou, Y.; Stanciu, L.; Stach, E. a; Xie, J. Graphene-Modified Nanostructured Vanadium Pentoxide Hybrids with Extraordinary Electrochemical Performance for Li-Ion Batteries. *Nat. Commun.* **2015**, *6*, 6127 DOI: 10.1038/ncomms7127.

(9) Goodenough, J. B. The Two Components of the Crystallographic Transition in VO_2. *J. Solid State Chemistry*. 1971, 490–500.

(10) Natelson, D. A Solid Triple Point. *Nature* **2013**, *500*, 408 DOI: 10.1038/500408a.

(11) O'Callahan, B. T.; Jones, A. C.; Hyung Park, J.; Cobden, D. H.; Atkin, J. M.; Raschke, M. B. Inhomogeneity of the Ultrafast Insulator-to-Metal Transition Dynamics of VO_2. *Nat. Commun.* **2015**, *6*, 6849 DOI: 10.1038/ncomms7849.

(12) Miller, M. J.; Wang, J. Influence of Grain Size on Transition Temperature of Thermochromic VO_2. *J. Appl. Phys.* **2015**, *117* (3) DOI: 10.1063/1.4906122.

(13) Dong, B.; Shen, N.; Cao, C.; Chen, Z.; Luo, H.; Gao, Y. Phase and Morphology Evolution of VO_2 Nanoparticles Using a Novel Hydrothermal System for Thermochromic Applications: The Growth Mechanism and Effect of Ammonium (NH_4^+). *RSC Adv.* **2016**, *6* (85), 81559–81568 DOI: 10.1039/C6RA14569H.

(14) Wang, S.; Liu, M.; Kong, L.; Long, Y.; Jiang, X.; Yu, A. Recent Progress in VO_2 Smart Coatings: Strategies to Improve the Thermochromic Properties. *Prog. Mater. Sci.* **2016**, *81*, 1–54 DOI: 10.1016/j.pmatsci.2016.03.001.

(15) Jian, J.; Zhang, W.; Jacob, C.; Chen, A.; Wang, H.; Huang, J.; Wang, H. Roles of Grain Boundaries on the Semiconductor to Metal Phase Transition of VO_2 Thin Films. *Appl. Phys. Lett.* **2015**, *107* (10), 102105 DOI: 10.1063/1.4930831.

(16) Schwingenschlögl, U.; Eyert, V. The Vanadium Magnéli Phases V_nO_{2n-1}. *Ann. Phys.* **2004**, *13* (9), 475–510 DOI: 10.1002/andp.200410099.

(17) Kotliar, G.; Vollhardt, D. Strongly Correlated Materials: Insights From Dynamical Mean-Field Theory. *Phys. Today* **2004**, *57*, 53–59 DOI: 10.1063/1.1712502.

(18) Hu, Y.; Shi, Q.; Huang, W.; Zhu, H.; Yue, F.; Xiao, Y.; Liang, S.; Lu, T. Preparation and Phase Transition Properties of Ti-Doped VO_2 Films by Sol–gel Process. *J. Sol-Gel Sci. Technol.* **2016**, *78* (1), 19–25 DOI: 10.1007/s10971-015-3913-z.

(19) Charipar, N. A.; Kim, H.; Breckenfeld, E.; Charipar, K. M.; Mathews, S. A.; Piqué, a. Polycrystalline VO_2 Thin Films via Femtosecond Laser Processing of Amorphous VO_x. *Appl. Phys. A Mater. Sci. Process.* **2016**, *122* (5) DOI: 10.1007/s00339-016-0034-7.

(20) Powell, M. J.; Quesada-Cabrera, R.; Taylor, A.; Teixeira, D.; Papakonstantinou, I.; Palgrave, R. G.; Sankar, G.; Parkin, I. P. Intelligent Multifunctional $VO_2/SiO_2/TiO_2$ Coatings for Self-Cleaning, Energy-Saving Window Panels. *Chem. Mater.* **2016**, *28* (5), 1369–1376 DOI: 10.1021/acs.chemmater.5b04419.

(21) Sobhan, M. A.; Kivaisi, R. T.; Stjerna, B.; Granqvist, C. G. Thermochromism of Sputter Deposited $W_xV_{1-x}O_2$ Films. *Sol. Energy Mater. Sol. Cells* **1996**, *44* (4), 451–455 DOI: 10.1016/S0927-0248(95)00051-8.

(22) Singh, T.; Wang, S.; Aslam, N.; Zhang, H.; Hoffmann-Eifert, S.; Mathur, S. Atomic Layer Deposition of Transparent VO_x Thin Films for Resistive Switching Applications. *Chem. Vap. Depos.* **2014**, *20*, 291–297 DOI: 10.1002/cvde.201407122.

(23) Wang, X.; Guo, Z.; Gao, Y.; Wang, J. Atomic Layer Deposition of Vanadium Oxide Thin Films from Tetrakis(dimethylamino)vanadium Precursor. *J. Mater. Res.* **2016**, 1–8 DOI: 10.1557/jmr.2016.303.

(24) Mathur, S.; Ruegamer, T.; Grobelsek, I. Phase-Selective CVD of Vanadium Oxide Nanostructures. *Chem. Vap. Depos.* **2007**, *13* (1), 42–47 DOI: 10.1002/cvde.200606578.

(25) Naik, A. J. T.; Bowman, C.; Panjwani, N.; Warwick, M. E. A.; Binions, R. Electric Field Assisted Aerosol Assisted Chemical Vapour Deposition of Nanostructured Metal Oxide Thin Films. *Thin Solid Films* **2013**, *544*, 452–456 DOI: 10.1016/j.tsf.2013.02.082.

(26) Manning, T.; Parkin, I.; Pemble, M.; Sheel, D.; Vernardou, D. Intelligent Window Coatings: Atmospheric Pressure Chemical Vapour Deposition of Tungsten-Doped Vanadium Dioxide. *Chem. Mater.* **2004**, *16* (13), 744–749 DOI: 10.1039/b205427m.

(27) Granqvist, C. G. Recent Progress in Thermochromics and Electrochromics: A Brief Survey. *Thin Solid Films* **2015**, *614*, 90–96 DOI: 10.1016/j.tsf.2016.02.029.

(28) Louloudakis, D.; Vernardou, D.; Spanakis, E.; Suchea, M.; Kenanakis, G.; Pemble, M.; Savvakis, K.; Katsarakis, N.; Koudoumas, E.; Kiriakidis, G. Atmospheric Pressure Chemical Vapor Deposition of Amorphous Tungsten Doped Vanadium Dioxide for Smart Window Applications. *Adv. Mater. Lett.* **2016**, *7* (3), 192–196 DOI: 10.5185/amlett.2016.6024.

(29) Bodurov, G.; Ivanova, T.; Abrashev, M.; Nenova, Z.; Gesheva, K. Thin Film Optical Coatings of Vanadium Oxide and Mixed Tungsten/vanadium Oxide Deposited by APCVD Employing Precursors of Vanadyl Acetylacetonate and a Mixture with Tungsten Hexacarbonyl. *Phys. Procedia* **2013**, *46*, 127–136 DOI: 10.1016/j.phpro.2013.07.054.

(30) Vernardou, D.; Louloudakis, D.; Spanakis, E.; Katsarakis, N.; Koudoumas, E. Amorphous Thermochromic VO_2 Coatings Grown by APCVD at Low Temperatures. *Adv. Mater. Lett.* **2015**, *6* (7), 660–663 DOI: 10.5185/amlett.2015.5810.

(31) Piccirillo, C.; Binions, R.; Parkin, I. Synthesis and Functional Properties of Vanadium Oxides: V_2O_3, VO_2, and V_2O_5 Deposited on Glass by Aerosol-Assisted CVD. *Chem. Vap. Depos.* **2007**, *13*, 145–151 DOI: 10.1002/cvde.200606540.

(32) Niklasson, G. a; Li, S.-Y.; Granqvist, C. G. Thermochromic Vanadium Oxide Thin Films: Electronic and Optical Properties. *J. Phys. Conf. Ser.* **2014**, *559*, 012001 DOI: 10.1088/1742-6596/559/1/012001.

(33) Sun, Y.; Xiao, X.; Xu, G.; Dong, G.; Chai, G.; Zhang, H.; Liu, P.; Zhu, H.; Zhan, Y. Anisotropic Vanadium Dioxide Sculptured Thin Films with Superior Thermochromic Properties. *Sci. Rep.* **2013**, *3*, 2756 DOI: 10.1038/srep02756.

(34) Xu, Y.; Huang, W.; Shi, Q.; Zhang, Y.; Wu, J.; Song, L. Porous Nano-Structured VO_2 Films with Different Surfactants: Synthesis Mechanisms, Characterization, and Applications. *J. Mater. Sci. Mater. Electron.* **2013**, *24* (10), 3823–3829 DOI: 10.1007/s10854-013-1324-x.

(35) Warwick, M. E. A; Ridley, I.; Binions, R. Thermochromic Vanadium Dioxide Thin Films from Electric Field Assisted Aerosol Assisted Chemical Vapour Deposition. *Surf. Coat. Technol.* **2013**, *230*, 163–167 DOI: 10.1016/j.surfcoat.2013.06.077.

(36) Warwick, M. E. A.; Ridley, I.; Binions, R. Thermochromic Vanadium Dioxide Thin Films Prepared by Electric Field Assisted Atmospheric Pressure Chemical Vapour Deposition for Intelligent Glazing Application and Their Energy Demand Reduction Properties. *Sol. Energy Mater. Sol. Cells* **2016**, *157*, 686–694 DOI: 10.1016/j.solmat.2016.07.031.

(37) Mathur, S.; Kuhn, P. CVD of Titanium Oxide Coatings: Comparative Evaluation of Thermal and Plasma Assisted Processes. *Surf. Coatings Technol.* **2006**, *201* (3-4), 807–814 DOI: 10.1016/j.surfcoat.2005.12.039.

(38) Müller, R.; Hernandez-Ramirez, F.; Shen, H.; Du, H.; Mader, W.; Mathur, S. Influence of Precursor Chemistry on Morphology and Composition of CVD-Grown SnO_2 Nanowires. *Chem. Mater.* **2012**, *24* (21), 4028–4035 DOI: 10.1021/cm300913h.

(39) Thomas, T.; Blackman, C. S.; Parkin, I. P.; Carmalt, C. J. Atmospheric Pressure Chemical Vapour Deposition of Vanadium Arsenide Thin Films via the Reaction of VCl_4 or $VOCl_3$ with $tBuAsH_2$. *Thin Solid Films* **2013**, *537*, 171–175 DOI: 10.1016/j.tsf.2013.04.144.

(40) Bradley, D. C.; Mehta, M. L. Alkoxides of Vanadium (IV). *Can. J. Chem.* **1962**, *40* (6), 1183–1188 DOI: 10.1139/v62-180.

(41) Bradley, D. C.; Moss, R. H.; Sales, K. D. Electron Spin Resonance Studies on Quadrivalent Vanadium Compounds. *J. Chem. Soc. D Chem. Commun.* **1969**, *11* (21), 1255 DOI: 10.1039/c29690001255.

(42) Nunes, G. G.; Friedermann, G. R.; dos Santos, J. L. B.; Herbst, M. H.; Vugman, N. V.; Hitchcock, P. B.; Leigh, G. J.; Sá, E. L.; da Cunha, C. J.; Soares, J. F. The First Thermochromic vanadium(IV) Alkoxide System. *Inorg. Chem. Commun.* **2005**, *8* (1), 83–88 DOI: 10.1016/j.inoche.2004.11.011.

(43) Westrup, K. C. M.; Gregório, T.; Stinghen, D.; Reis, D. M.; Hitchcock, P. B.; Ribeiro, R. R.; Barison, A.; Back, D. F.; de Sá, E. L.; Nunes, G. G.; Soares, J. F. Non-Oxo vanadium(IV) Alkoxide Chemistry: Solid State Structures, Aggregation Equilibria and Thermochromic Behaviour in Solution. *Dalton Trans.* **2011**, *40* (13), 3198–3210 DOI: 10.1039/c0dt01547d.

(44) Haaland, A.; Rypdal, K.; Volden, H. V.; Andersen, R. A. Molecular Structures of titanium(IV) and vanadium(IV) Amides and Alkoxides. *J. Chem. Soc., Dalton Trans.* **1992**, 891-895 DOI: 10.1039/DT9920000891.

(45) Yang, M.; Yang, Y.; Bin Hong; Wang, L.; Hu, K.; Dong, Y.; Xu, H.; Huang, H.; Zhao, J.; Chen, H.; Song, L.; Ju, H.; Zhu, J.; Bao, J.; Li, X.; Gu, Y.; Yang, T.; Gao, X.; Luo, Z.; Gao, C. Suppression of Structural Phase Transition in VO2 by Epitaxial Strain in Vicinity of Metal-Insulator Transition. *Sci. Rep.* **2016**, *6* (1), 23119 DOI: 10.1038/srep23119.

(46) Breckenfeld, E.; Kim, H.; Burgess, K.; Charipar, N.; Cheng, S.-F.; Stroud, R.; Piqué, A. Strain Effects in Epitaxial VO_2 Thin Films on Columnar Buffer-Layer TiO_2/Al_2O_3 Virtual Substrates. *ACS Appl. Mater. Interfaces* **2017**, *9*, 1577−1584 DOI: 10.1021/acsami.6b13112.

(47) Surnev, S.; Ramsey, M. G.; Netzer, F. P. Vanadium Oxide Surface Studies. *Prog. Surf. Sci.* **2003**, *73* (4-8), 117–165 DOI: 10.1016/j.progsurf.2003.09.001.

(48) Demeter, M.; Neumann, M.; Reichelt, W. Mixed-Valence Vanadium Oxides Studied by XPS. *Surf. Sci.* **2000**, *454* (1), 41–44 DOI: 10.1016/S0039-6028(00)00111-4.

(49) Brockman, J.; Aetukuri, N. P.; Topuria, T.; Samant, M. G.; Roche, K. P.; Parkin, S. S. P. Increased Metal-Insulator Transition Temperatures in Epitaxial Thin Films of V_2O_3 Prepared in Reduced Oxygen Environments. *Appl. Phys. Lett.* **2011**, *98* (15), 152105 DOI: 10.1063/1.3574910.

(50) Fei, H.; Ding, X.; Wei, M.; Wei, K. Facile Synthesis of Montroseite VOOH, Paramontroseite VO_2 and V_2O_3-VO_2 Carbonaceous Core-Shell Microspheres. *Solid State Sci.* **2011**, *13* (11), 2049–2054 DOI: 10.1016/j.solidstatesciences.2011.09.009.

(51) Xu, Y.; Zheng, L.; Xie, Y. From Synthetic Montroseite VOOH to Topochemical Paramontroseite VO_2 and Their Applications in Aqueous Lithium Ion Batteries. *Dalt. Trans.* **2010**, *39*, 10729–10738 DOI: 10.1039/c0dt00715c.

(52) Stoe & Cie GmbH, Darmstadt Deutschland, X-RED32 1.31 (2005) & X-SHAPE 1.06 (1999).

(53) Farrugia, L. J. WinGX suite for small-molecule single-crystal crystallography. *J. Appl. Crystallogr.* **1999**, *32*, 837-838.

(54) Altomare, A.; Cascarano, G; Giacovazzo, C; Guagliardi, A. SIRPOW. 92–a program for automatic solution of crystal structures by direct methods optimized for powder data. *J. Appl. Crystallogr.* **1994**, *27*, 435.

(55) Sheldrick, G. M. A short history of SHELX. *Acta Crystallogr., Sect. A: Found. Crystallogr.* **2008**, *64*, 112-122.

(56) Spek, A. L. Single-crystal structure validation with the program PLATON. *J. Appl. Crystallogr.* **2003**, *36*, 7-13.

Table of Content